Negative exciton mass in ZnCdSe/ZnSSe superlattices observed by excitonic polariton Raman scattering



1999 J. Phys.: Condens. Matter 11 1735

(http://iopscience.iop.org/0953-8984/11/7/007)

J. Phys.: Condens. Matter **11** (1999) 1735–1744. Printed in the UK PII: S0953-8984(99)95521-2

# Negative exciton mass in ZnCdSe/ZnSSe superlattices observed by excitonic polariton Raman scattering

A Je Semjonow, U W Pohl† and R Engelhardt

Technische Universität Berlin, Institut für Festkörperphysik, Sekretariat PN 6-1, Hardenbergstrasse 36, D-10623 Berlin, Germany

Received 1 July 1998, in final form 17 November 1998

**Abstract.** Resonant Raman scattering of excitonic polaritons at LO phonons in ZnCdSe/ZnSSe superlattices at room temperature reveals strong spatial dispersion effects near the transverse excitonic resonance frequency $\omega_{\mathrm{T}}$. For incident photon energies below $\omega_{\mathrm{T}}$, the LO phonon anti-Stokes frequency shifts exceed the Stokes shifts, while the inverse relation holds above $\omega_{\mathrm{T}}$. All experimental results can be well described in the excitonic polariton formalism in terms of exciton branches with positive and negative excitonic masses above and below $\omega_{\mathrm{T}}$, respectively, and an additional damping parameter.

## 1. Introduction

Raman scattering is expected to be resonantly enhanced when the energy of the incident or scattered light approaches the energy of an electronic or excitonic transition in the medium [1]. Over a wide energy range around the excitonic resonance $\omega_{\mathrm{T}}$, the exciton admixture with the propagating light is almost complete, and the region of the resonance frequency is determined not by the longitudinal–transverse splitting $\omega_{\mathrm{LT}}$, but by [2]

$$\omega_{\mathrm{c}} = \sqrt{\omega_{\mathrm{LT}}\omega_{\mathrm{T}}}. \tag{1}$$

The polariton wave function with the frequency $\omega_{\mathrm{i}}$ has a mixed character in the region $|\omega_{\mathrm{i}} - \omega_{\mathrm{T}}| \leqslant \omega_{\mathrm{c}}$, while its dispersion appears almost unperturbed beyond $|\omega_{\mathrm{i}} - \omega_{\mathrm{T}}| \geqslant \omega_{\mathrm{LT}}$.

Raman scattering near $\omega_{\mathrm{LT}}$ is usually well described by a positively bent polariton dispersion, i.e. a positive exciton mass. In the case where $\omega_{\mathrm{i}} < \omega_{\mathrm{T}}$, where exciton branches with positive excitonic mass are absent, excitons may in principle also exist that are theoretically described by a negative mass [3], i.e. a negatively bent dispersion branch. Large negative masses of holes were especially proposed for II–VI semiconductors. Corresponding Raman resonances have, however, not yet been reported. If a negative branch exists, resonances are expected for scattering with phonons of sufficiently large wave vector. In pure bulk samples and at the low measuring temperatures usually used, the observed phonons have small wave vectors, because only phonon contributions near the $\Gamma$ point are excited. To observe possible resonances of a negative-mass branch, the temperature must thus be raised. At $\sim$100 K, phonons with sufficiently large wave vectors for the phenomena described below to be observable already exist. At temperatures exceeding the Debye temperature $T_{\mathrm{D}} \simeq 1.44\omega_{\mathrm{LO}}$ ($T_{\mathrm{D}} \simeq 350$ K for ZnSe crystals), phonons can be found over the entire Brillouin zone.

† Author to whom any correspondence should be addressed. Fax: +49 30 314 22064; e-mail address: pohl@physik.tu-berlin.de.

0953-8984/99/071735+10$19.50  

Since excitons in bulk samples dissociate at increased temperatures, layered structures with quantum wells (QWs) are more suitable. The confinement potential allows the observation of free excitons even at room temperature [4]. The localization in QWs strengthens the electron–hole Coulomb interaction, resulting in an increased binding energy and oscillator strength of QW excitons [5]. Confinement effects also change the selection rules for phonons [6], and phonons with larger wave vectors are involved in the exciton–phonon interaction. In addition, spatial dispersion effects may appear, as reported for resonant scattering at acoustic phonons [7–9] and at two-phonon states involving an acoustic and an optical phonon [10, 11]. We therefore investigated superlattices of II–VI semiconductors by means of resonant Raman scattering at room temperature.

## 2. Experimental conditions

The samples investigated were grown on GaAs(001) by low-pressure MOVPE using DMZn-TEN, DTBSe, tBSH, and DMCd precursors. The structures consist of tenfold ZnCdSe/ZnSSe superlattices each grown on a 5 nm ZnSe buffer and covered with a 10 nm ZnSSe cap which has the same sulphur content as the barriers. The periodicity and composition of these superlattices, as determined by x-ray diffraction, are as follows: 2.9 nm compressively strained $Zn_{0.79}Cd_{0.21}Se$ quantum wells are strain compensated by $ZnS_{0.14}Se_{0.86}$ barrier layers 15 nm thick under tensile strain. The remaining lattice mismatch of the whole stack is less than 0.1% with respect to the GaAs substrate.

The Raman spectra were recorded at room temperature in the backscattering geometries $z(yx)\bar{z}$ (allowed) and $z(xx)\bar{z}$ (forbidden), with the incident and scattered light nearly perpendicular to the (001) sample surface ($z \equiv [001]$, $x \equiv [110]$, $y \equiv [1\bar{1}0]$). The spectra presented were recorded in the $z(xx)\bar{z}$ geometry. Identical phonon frequencies were observed in $z(yx)\bar{z}$ geometry. The scattered light was analysed by a Dilor-XY spectrometer which was calibrated using a Si monocrystal before each spectrum was taken. The spectral resolution was better than 0.5 $cm^{-1}$. We used lines of $Ar^+$ and $Kr^+$ lasers with a typical power density at the sample of $5 \times 10^3$ W $cm^{-2}$.

## 3. Experimental results

The ZnCdSe/ZnSSe superlattice exhibits a strong exciton luminescence under UV excitation, peaking near 2.7 eV at low temperatures; see figure 1. The structure of the luminescence band is thought to originate from thickness fluctuations of the ZnCdSe QWs. The two peaks denoted a and b agree well with electron–heavy-hole transition energies calculated for $Zn_{0.79}Cd_{0.21}Se$ QWs 10 and 12 monolayers thick, respectively. With increasing temperature, both peaks show a bandgap-related red-shift which can be well fitted by Varshni's relation [12]. The excitonic resonance observed at room temperature appears at $\omega_T = 20\,935$ $cm^{-1}$ (477.7 nm).

Raman spectra excited at different frequencies $\omega_i$ are given in figure 2. To assign the observed phonons, we compared the LO phonon frequencies of ternary alloys for the compositions given in the superlattice $Zn_{1-x}Cd_xSe$ QWs ($x = 0.2$) and $ZnS_xSe_{1-x}$ barriers ($x = 0.14$) with reported data. In bulk ZnCdSe crystals with $x = 0.2$ Cd content, the ZnSe-like LO phonon appears at $\omega_{LO} = 246$ $cm^{-1}$ [13]. In $ZnS_xSe_{1-x}$ layers with a sulphur content $x = 0.14$, a frequency $\omega_{LO} = 249$ $cm^{-1}$ has been reported for ZnSe-like LO phonons [14]. In our measurements, the position of ZnSe-like LO phonons is $\omega_{LO} = 244.7$ $cm^{-1}$ for non-resonant conditions ($\lambda_i = 515$ and 501 nm) and $\omega_{LO} = 251.7$ $cm^{-1}$ at resonance. The additional weak peaks marked in figure 2 can be assigned to CdSe and ZnS lattice vibrations

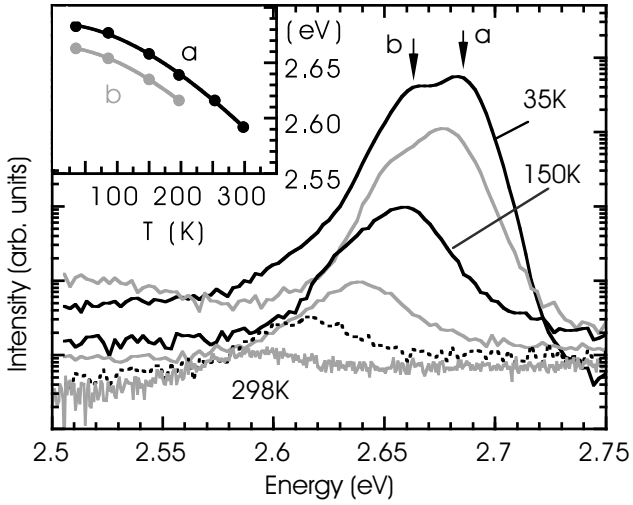


**Figure 1.** The excitonic luminescence of the ZnCdSe/ZnSSe superlattice, excited at 3.81 eV. The temperature dependence of the two maxima is shown in the inset; the solid traces are fits according to Varshni's relation.

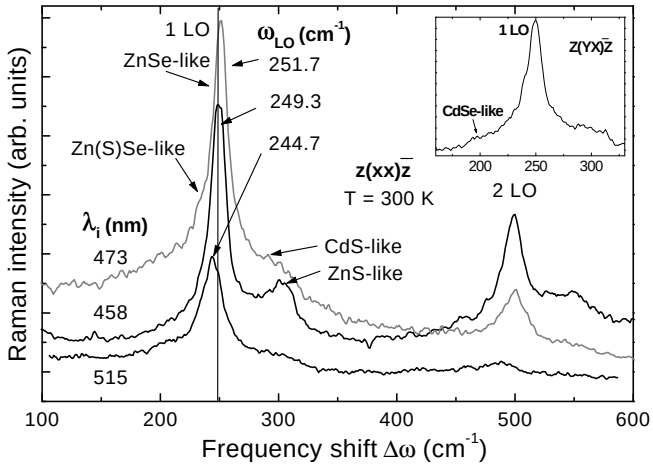


**Figure 2.** Raman spectra of the ZnCdSe/ZnSSe superlattice, recorded for different excitation wavelengths $\lambda_i$ in $z(xx)\bar{z}$ geometry at room temperature. The vertical line near 250 $cm^{-1}$ is a guide to help one to recognize differences in the 1LO phonon energies.

resulting from the one-mode behaviour in the wells [13] and the two-mode behaviour in the barriers [14], respectively. In addition, a weak CdS-like phonon is observed under resonant conditions. This mode is thought to originate from Cd diffusion into the barrier material due to the high diffusivity of Cd [15].

The phonon modes which appear in addition to the ZnSe-like mode in figure 2 are not assigned to confined phonon modes of the superlattice. The respective frequencies do not coincide with the observed frequencies. This is thought to be connected with an insufficient quality of the interfaces between the ZnCdSe QWs and the ZnSSe barriers, because the appearance of such modes depends sensitively on the interfaces being sufficiently smooth.

Since the superlattice is transparent for a non-resonant excitation, we observe away from resonance only Raman spectra originating from the ZnSSe layers which are thicker ($10 \times 15$ nm) than the quantum wells ($10 \times 2.9$ nm). The frequency of the ZnSe-like phonon in the ZnSSe is, however, observed at 244.7 $cm^{-1}$ instead of the frequency 249 $cm^{-1}$ reported for thicker layers [14]. To explain the apparent shift of the ZnSe-like LO phonon, the influence of strain in the layers has to be considered. If we assume the compressive strain in the superlattice to be completely confined to the ZnCdSe QW layers and all of the tensile strain to the ZnSSe barriers, we can apply the standard approach for strain-induced Raman shifts [16, 17] given by $\omega_{LO}(\varepsilon) = \omega_{LO}(0)[1 - (2.35 \pm 0.4)\varepsilon]$ with the material constants of ZnSe. We obtain an in-plane strain $\varepsilon = -1.0\%$ for the QWs and $\varepsilon = +0.7\%$ for the barriers. This is in good agreement with the results of our x-ray measurements.

**Table 1.** 1LO phonon frequencies in quantum wells and barriers of a ZnCdSe/ZnSSe superlattice at room temperature, in comparison with the results for $Zn_{0.79}Cd_{0.21}Se$ and $ZnS_{0.14}Se_{0.86}$ bulk mixed crystals. Strains calculated from the superlattice phonon frequencies are given in the first and last columns.

| Strain in well (%) | $\omega_{LO}$ ($cm^{-1}$) in $Zn_{0.79}Cd_{0.21}Se$ | | $\omega_{LO}$ ($cm^{-1}$) in $ZnS_{0.14}Se_{0.86}$ | | Strain in barrier (%) |
|---|---|---|---|---|---|
| | Quantum well | Bulk | Barrier | Bulk | |
| −1.0 ZnSe-like | $251.7 \pm 0.5$ | 246[a] | $244.7 \pm 0.5$ | 249[b] | + 0.7 ZnSe-like |
| −0.9 CdSe-like | $198 \pm 2$ | 194[a] | $302 \pm 2$ | 307[b] | + 0.8 ZnS-like |
| | | | $294 \pm 2$ | 304[c] | + 1.4 CdS-like |

[a] Reference [13].
[b] Reference [14].
[c] Reference [19].

If the excitation energy approaches the exciton resonance, the QW phonons show a continuous increase of the LO frequency shift in Raman Stokes spectra up to $\omega_{LO} = 251.7\ cm^{-1}$ for $\lambda_i = 473$ nm, and up to $\omega_{LO} = 248.9\ cm^{-1}$ for $\lambda_i = 483$ nm in anti-Stokes Raman spectra, compared to $\omega_{LO} = 246\ cm^{-1}$ for bulk mixed ZnCdSe crystals. This finding supports our assumption of compressive strain in the QWs and tensile strain in the barriers. The energies of CdSe-like, ZnS-like, and CdS-like LO phonons confirm this picture of strain. The frequency positions of the observed phonons in the QWs and in the barriers with respect to their positions in bulk mixed crystals and the calculated strains are shown in table 1. The decrease of the LO frequency of the CdS-like phonons relative to that in bulk crystals indicates that these phonons belong to the barriers.

Differences in resonant Raman spectra which are excited with energies above and below the exciton resonance $\omega_T$ are shown in figure 3. In all of the spectra the maxima of the phonon lines are resonantly enhanced if the energy of the excitonic peak coincides with the energy of a LO phonon peak. For an excitation with $\lambda_i = 458$ nm, the Stokes 3LO and 4LO phonons have thus maximal intensity, because the exciton resonance $\omega_T$ appears between these peaks (figure 3(a)). In addition, the weak ZnS-like phonon on the high-energy side of the ZnSe-like 1LO, 2LO, and 3LO phonons is well resolved in this case. For $\omega_i$ below $\omega_T$, anti-Stokes lines are more intensive than Stokes lines, due to their smaller energy separation from the exciton resonance; see figure 3(b) and table 2. From the Raman spectra, an exciton resonance $\omega_T = 20\,934\ cm^{-1}$ is derived. The value agrees well with that from the photoluminescence

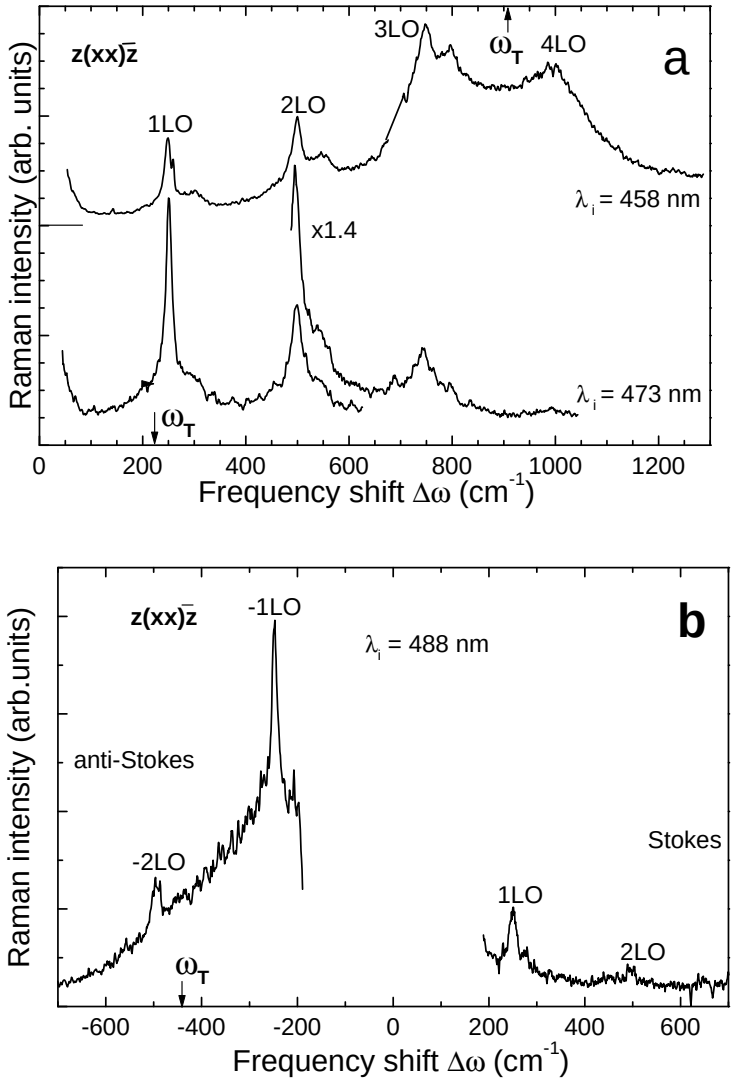


**Figure 3.** Resonant Raman spectra excited with energies (a) above and (b) below the excitonic resonance $\omega_{\mathrm{T}}$. The excitonic resonance is marked by arrows.

measurements.

Inserting this $\omega_{\mathrm{T}}$-value and a longitudinal–transverse splitting $\omega_{\mathrm{LT}} = 11.7$ cm$^{-1}$ [8] into equation (1), resonances between excitons and LO phonons can be expected in a frequency region $\omega_{\mathrm{c}} = |\omega_{\mathrm{i}} - \omega_{\mathrm{T}}| \leqslant 495$ cm$^{-1}$. We studied Raman spectra associated with LO phonons over a wide frequency range, $-793$ cm$^{-1}$ $< (\omega_{\mathrm{T}} - \omega_{\mathrm{i}}) <$ +905 cm$^{-1}$, as listed in table 2. The observed frequency deviation from the usual, non-resonant position of LO phonons at 244.7 cm$^{-1}$ increases with the incident excitation energy and reaches approximately +7 cm$^{-1}$ for $\lambda_{\mathrm{i}} = 473$ nm; see figure 4. It can be recognized that the anti-Stokes frequency shifts exceed the Stokes shifts for incident photon energies below $\omega_{\mathrm{T}}$, while the relation is reversed above $\omega_{\mathrm{T}}$. Furthermore, the increase of the LO phonon frequency observed at lower excitation

**Table 2.** Resonance shifts of the incident laser light ($\omega_i$), Stokes ($\omega_{St}$), and anti-Stokes ($\omega_{aSt}$) Raman frequencies ($\omega_{St} = \omega_i - \omega_{nLO}$, $\omega_{aSt} = \omega_i + \omega_{nLO}$, with the order $n = 1, 2, 3, 4$ of multiphonon scattering) with respect to the excitonic resonance $\omega_T$. The last four columns give the resulting deviations of 1LO ZnSe-like phonon frequencies ($\Delta\omega$) from the non-resonant position $\omega_{1LO} = 245$ cm$^{-1}$. Computed data were obtained for the parameters $m_+^* = 0.65\ m_0$, $m_-^* = -1.9\ m_0$, and $\gamma = 40$ cm$^{-1}$. ('Res. shift' stands for resonance shift.)

| Laser line $\lambda_i$ (nm) | Res. shift $(\omega_i - \omega_T)$ (cm$^{-1}$) | Res. shift $(\omega_{St} - \omega_T)$ (cm$^{-1}$) | Res. shift $(\omega_{aSt} - \omega_T)$ (cm$^{-1}$) | $\Delta\omega_{St}$ (cm$^{-1}$) | | $\Delta\omega_{aSt}$ (cm$^{-1}$) | |
|---|---|---|---|---|---|---|---|
| | | | | Experiment | Theory | Experiment | Theory |
| 457.9 | + 905 | −75 ($\omega_{4LO}$)<br>+ 170 ($\omega_{3LO}$) | | 4.5 | 4.9 | 2.3 | 1.3 |
| 472.7 | + 221 | −24 ($\omega_{1LO}$)<br>−269 ($\omega_{2LO}$) | + 466 ($\omega_{1LO}$) | 7 | 7.6 | 1.6 | 1.0 |
| 476.5 | + 52 | −193 ($\omega_{1LO}$)<br>−438 ($\omega_{2LO}$) | + 297 ($\omega_{1LO}$) | 5.3 | 5.2 | 3.3 | 2.4 |
| 482.5 | −209 | −454 ($\omega_{1LO}$) | + 36 ($\omega_{1LO}$)<br>+ 271 ($\omega_{2LO}$) | 3.3 | 3.2 | 4.2 | 4.8 |
| 488.0 | −442 | | −197 ($\omega_{1LO}$)<br>+ 48 ($\omega_{2LO}$) | 1.3 | 1.0 | 3.3 | 3.3 |
| 496.5 | −793 | | + 187 ($\omega_{4LO}$)<br>−58 ($\omega_{3LO}$) | 0.3 | 0.5 | 2 | 1.5 |

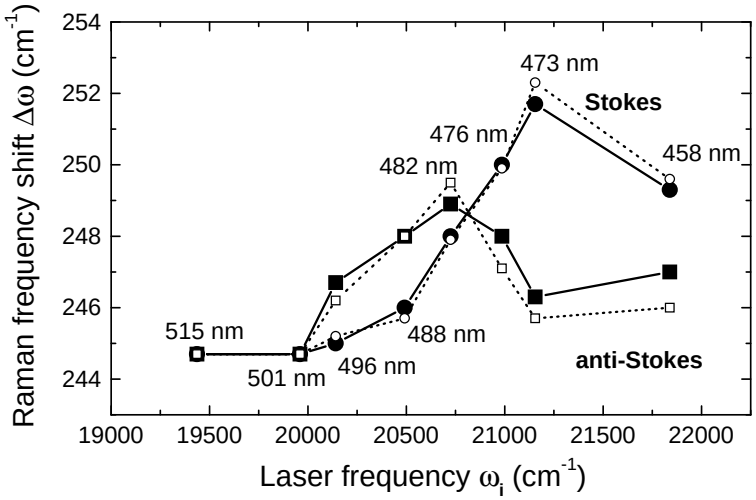


**Figure 4.** Stokes (circles) and anti-Stokes (squares) Raman frequency shifts as a function of the excitation energy $\omega_i$. Full squares and circles represent experimental results (solid lines); the positions of the open symbols indicate resonance shifts calculated using equation (4) (dashed lines). The spectral accuracy of the mode frequency determination is $\pm 0.5$ cm$^{-1}$.

energies is not continued at the highest excitation energy measured. Thus for $\lambda_i = 458$ nm, where the laser line is no longer in resonance, the frequency shift of the ZnSe-like phonons is decreased in comparison with $\lambda_i = 473$ nm.

The LO frequency shift pattern cannot be explained solely by strain effects. In QW structures, strain induces a shift to the high-frequency side, as reported for ZnCdSe/ZnSe QWs

[17]. The effect, however, is the same for both Stokes and anti-Stokes components. In our measurements, the positions of Stokes and anti-Stokes lines are not only different, but change their relative positions according to the position of the incident light energy with respect to the excitonic resonance $\omega_T$.

If light waves propagating in a crystal become in resonance with an intrinsic transverse polarized excitation such as optical phonons or excitons, waves of mixed light polarization are formed. The dispersion curve of such waves corresponds to a continuous transition from the photon dispersion curve in the crystal to the dispersion curve of excitons within an energy range of about 25 $cm^{-1}$ around the resonance $\omega_T$ (a region generally studied by means of resonant Brillouin scattering). Thus photons in the crystal and excitons form a single dispersion curve, and excitations corresponding to this dispersion curve result in excitonic polaritons. In the region of parabolic dispersion, polaritons can be regarded as quasiparticles which have a certain effective mass and kinetic energy. In the following section we describe our experimental results in the framework of the excitonic polariton formalism in terms of exciton branches with positive and negative excitonic masses above and below $\omega_T$, respectively, and an additional damping parameter.

## 4. Discussion

The experimentally observed dependency of LO phonon Stokes Raman lines on the laser energy shown in figure 4 can, in the resonance region, be approximated by the parabolic dependence

$$\omega(K) = \omega_{LO} + A\bar{h}(K - K_0)^2/2m_0. \tag{2}$$

where $m_0$ is the free-electron mass, $\bar{h}$ is Planck's constant, and $A$ is a dimensionless parameter describing the parabolic bending. $K$ and $K_0$ are the wave vectors of the phonon and the light, respectively ($K_0 \simeq 0$), and $\omega_{LO}$ denotes the LO phonon frequency away from resonance. We assume—as was shown to be reasonable in reference [18]—that

$$K v_X = \omega_{LO} \qquad \text{and} \qquad m^* v_X^2/2 = \bar{h}(\omega_i - \omega_T) \tag{3}$$

where $v_X$ is the exciton velocity, $\omega_i$ the frequency of the incident light, $\omega_T$ the position of the exciton peak at room temperature, and $m^*$ the excitonic mass. Stokes and anti-Stokes resonances are obtained from equations (2) and (3), yielding

$$(\omega_{St}(K) - \omega_{LO})/\omega_{LO} = A(m^*/m_0)(\omega_{LO}/(\omega_i - \omega_T) + \omega_{LO}/(\omega_{St} - \omega_{T)})) \tag{4a}$$

$$(\omega_{aSt}(K) - \omega_{LO})/\omega_{LO} = A(m^*/m_0)(\omega_{LO}/(\omega_i - \omega_T) + \omega_{LO}/(\omega_{aSt} - \omega_{T)})). \tag{4b}$$

The subscripts St and aSt stand for Stokes and anti-Stokes, respectively; $\omega_i - \omega_T$ gives the frequency difference of the incident light from the excitonic resonance. According to equation (4), we obtain $m_+^* > 0$ and $\omega_{aSt} < \omega_{St}$ for $\omega_i > \omega_T$, because the position of $\omega_{St}$ is always closer to the resonance than the position of $\omega_{aSt}$. In contrast, for $\omega_i < \omega_T$ we obtain (if this branch exists) $m_-^* < 0$ ($\omega_{aSt} > \omega_{St}$), because the position of $\omega_{aSt}$ is always closer to the resonance than the position of $\omega_{St}$.

For the superlattice investigated, the bending parameter $A$ of equation (2) can be obtained from the resonant Stokes shifts, yielding $A = 7.5 \times 10^{-2}$. The exciton resonance $\omega_T$ at room temperature is taken from Raman spectra: $\omega_T = 20\,934$ $cm^{-1}$. Using equation (4) and the experimental data listed in table 2, we can calculate the Stokes and anti-Stokes Raman shifts resulting from exciton polariton scattering at LO phonons. To obtain an optimal agreement with experimental results, an exciton absorption $\gamma$ was taken into account by extending $\omega_{LO}/(\omega_i - \omega_T)$ in equation (4) to $\omega_{LO}/(\omega_i - \omega_T + i\gamma)$. The results obtained with the parameters $m_+^* = 0.65\ m_0$, $m_-^* = -1.9\ m_0$, and $\gamma = 40$ $cm^{-1}$ agree quite well with the experimental results; see figure 4.

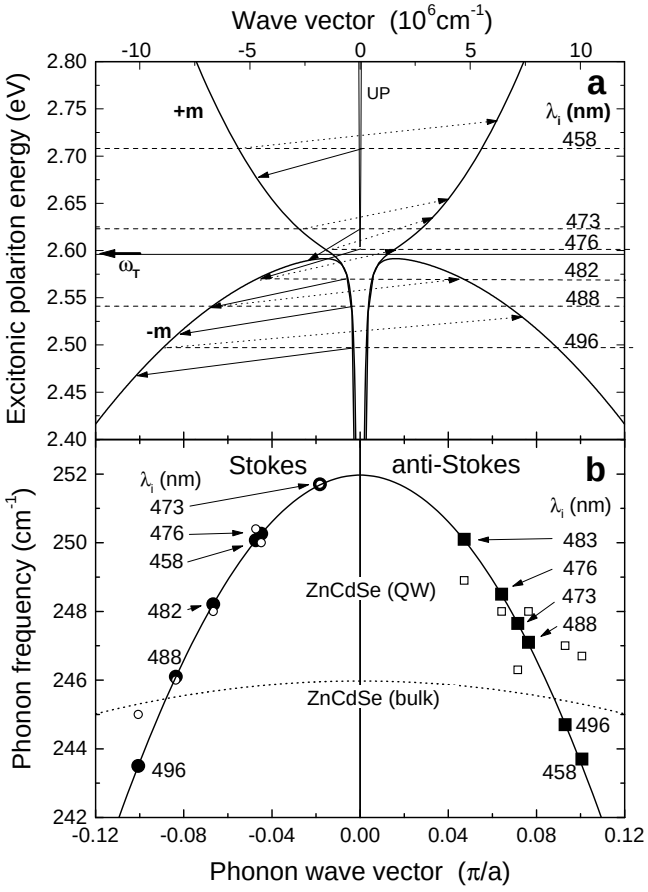


**Figure 5.** Dispersion curves for excitonic polaritons (a) and dispersion curves for ZnSe-like LO phonons (b) both in a ZnCdSe bulk crystal (biaxially strained like the QWs) with a $C$-fold-reduced wave vector (solid curve) and in an unstrained ZnCdSe bulk (dotted curve). The arrows in (a) represent Stokes (solid lines) and anti-Stokes (dotted lines) transitions measured in Raman spectra. 'UP' denotes an upper polariton branch. Open and solid circles and squares in (b) represent experimental and calculated frequencies of Stokes and anti-Stokes phonons, respectively.

For a more complete description of the experiments, the phonon wave vectors which interact with the excitonic polaritons in Raman scattering have to be considered. Using the dispersion relations for excitonic polaritons [8] with positive (for $\omega_\mathrm{i} > \omega_\mathrm{T}$) and negative (for $\omega_\mathrm{i} < \omega_\mathrm{T}$) exciton masses, and frequencies of initial and scattered excitonic polaritons, we can define the wave vectors of the particles (figure 5(a)). The effects of strain [17], confinement [20], and the usual conservation law for Stokes and anti-Stokes wave vectors are taken into account by a dispersion relation for ZnSe-like LO phonons in the form

$$\omega^2(K) = B_\varepsilon^2\{a + [a^2 - b(1 - \cos(\pi C K))]^{1/2}\}.$$

In this relation, $K$ is scaled in units of $2\pi/a_0$, $a = 3.2 \times 10^4$ cm$^{-2}$, and $b = 4.5 \times 10^8$ cm$^{-4}$. $B_\varepsilon$ is a strain-dependent parameter shifting $\omega$ at $K = 0$ from $\omega_{\varepsilon=0} = 246$ cm$^{-1}$ to $\omega_{\varepsilon=-0.01} = 252$ cm$^{-1}$. The factor $C$ was chosen as confinement parameter in the form $C = 2\pi \times 10^6/(d_1 + d_2) \approx 3.51$, where $d_1 + d_2$ is the superlattice period. Using this parameter, the experimental Stokes frequencies agree remarkably well with a dispersion curve of bulk

ZnCdSe (being strained like the QWs) with a $C$-fold-reduced wave vector. The direction of the phonon wave vector $\boldsymbol{K}$ can be derived from figure 5(a). The angle between $\boldsymbol{K}$ and the (001) surface is given by $\omega_{\mathrm{LO}}/|\boldsymbol{K}| \approx 0$. This means that the observed vector $\boldsymbol{K}_{\mathrm{ph}}$ lies in the plane of the QW.

The resulting phonon dispersion, and the experimental and computed wave vectors and frequencies are shown in figure 5(b). We obtain a good accordance between experimental and calculated phonon frequencies for Stokes processes, and a reasonable agreement for anti-Stokes scattering.

In *non-resonant* photon Raman scattering (in the backscattering configuration), the phonon wave vector ($q \approx 0$) is normal to the surface. In our case we have *resonance* scattering of excitonic polaritons at $A_1$ 'forbidden' phonons corresponding to the Fröhlich-interaction-induced scattering. In this case, the values of phonon wave vectors are defined by the values of excitonic polariton wave vectors which are identical to the in-plane phonon wave vectors $K_{\parallel} = K_{\mathrm{bulk}}/C$ with $C$ as defined above.

The consideration of an exciton branch with a negative exciton mass as proposed in reference [3] provides thus a complete description of all experimental findings within the framework of excitonic polaritons. As to the nature of negative excitonic masses, the appearance may be connected to the high compressive strain observed in the ZnCdSe QWs. Studies of the pressure dependence of the exciton binding energy in GaInAs QW structures [21] led to the conclusion of a pressure-induced negative hole mass. The main criteria allowing the observation of a negative exciton mass seem to be the following. First, the presence of resonance effects at $\omega_{\mathrm{i}} < \omega_{\mathrm{T}}$. Second, $\omega_{\mathrm{St}} \neq \omega_{\mathrm{aSt}}$: $\omega_{\mathrm{St}} < \omega_{\mathrm{aSt}}$ for $\omega_{\mathrm{i}} < \omega_{\mathrm{T}}$ and $\omega_{\mathrm{St}} > \omega_{\mathrm{aSt}}$ for $\omega_{\mathrm{i}} > \omega_{\mathrm{T}}$. Third, both phonons with sufficiently large wave vectors and excitons must exist at the measuring temperature.

## 5. Conclusions

Resonant Raman scattering of excitonic polaritons on optical (LO) phonons can be observed at room temperatures in ZnCdSe/ZnSSe superlattice structures. Resonance is possible if either the incident light or the scattered light fulfils Hopfield's criterion $|\omega_{\mathrm{i}} - \omega_{\mathrm{T}}| \leqslant \omega_{\mathrm{c}}$, where $\omega_{\mathrm{T}}$ is the transverse excitonic resonance, $\omega_{\mathrm{LT}}$ the longitudinal transverse splitting, and $\omega_{\mathrm{c}} = \sqrt{\omega_{\mathrm{LT}}\omega_{\mathrm{T}}} \simeq 495\ \mathrm{cm}^{-1}$ for ZnSe crystals. Spatial dispersion effects associated solely with optical LO phonons have been observed for the first time. The LO anti-Stokes frequency shifts exceed the Stokes shifts for incident photon energies $\omega_{\mathrm{i}}$ below $\omega_{\mathrm{T}}$, while the relation is reversed above $\omega_{\mathrm{T}}$. All of the experimental results are well described in the excitonic polariton picture using just three parameters, namely by branches with positive ($m_{+}^{*} = +0.65\, m_0$) and negative ($m_{-}^{*} = -1.9\, m_0$) excitonic masses above and below $\omega_{\mathrm{T}}$, respectively, and a damping parameter ($\gamma = 40\ \mathrm{cm}^{-1}$).

## References


[1] Klein M C, Hache F, Ricard D and Flytzanis C 1990 *Phys. Rev.* B **42** 11 123
[2] Hopfield J J 1969 *Phys. Rev.* **182** 945
[3] Cardona M 1963 *J. Phys. Chem. Solids* **24** 1543
[4] Dabbicco M, Lepore M, Cingolani R, Scamarcio G, Ferrara M and Suemune I 1992 *Semicond. Sci. Technol.* **7** 681
[5] Jorda S, Rössler U and Broido D 1993 *Phys. Rev.* B **48** 1669
[6] Campbell I H and Fauchet P M 1986 *Solid State Commun.* **58** 739
[7] Koteles E S and Winterling G 1979 *Phys. Rev.* B **20** 628

[8] Weisbuch C and Ulbrich R G 1987 *Light Scattering in Solids* vol 3, ed M Cardona and G Güntherodt (Berlin: Springer) p 207
[9] Sermage B and Fishman G 1979 *Phys. Rev. Lett.* **43** 1043
[10] Sermage B and Fishman G 1981 *Phys. Rev.* B **23** 5107
[11] Oka Y and Cardona M 1979 *Solid State Commun.* **30** 447
[12] Varshni Y P 1967 *Physica* **34** 149
[13] Valakh M Ja, Lisitsa M P, Pekar G S, Polysskii G N, Sidorenko V I and Yaremko A M 1982 *Phys. Status Solidi* b **113** 635
[14] Hayashi K, Sawaki N and Akasaki I 1991 *Japan J. Appl. Phys.* **30** 501
[15] Kuttler M, Strassburg M, Türck V, Heitz R, Pohl U W, Bimberg D, Kurtz E, Landwehr G and Hommel D 1996 *Appl. Phys. Lett.* **69** 2647
[16] Cerdeira F, Buchenauer C J, Pollak F H and Cardona M 1972 *Phys. Rev.* B **5** 580
[17] Pelekanos N T, Ding J, Hagerott M, Nurmikko A V, Luo H, Samarth N and Furdyna J K 1992 *Phys. Rev.* B **45** 6037
[18] Hamilton D C 1969 *Phys. Rev.* **188** 1221
[19] Leite R C C, Scott J F and Damen T C 1969 *Phys. Rev. Lett.* **22** 780
[20] Tishchenko V V, Raptis Y S, Anastassakis E and Bondar N V 1995 *Solid State Commun.* **96** 793
[21] Goñi A R, Syassen K, Zhang Y, Ploog K, Cantarero A and Cros A 1992 *Phys. Rev.* B **45** 6809